Design of Magneto-Optical Ring Isolator on SOI Based on the Finite-Element Method

P. Pintus, *Student Member, IEEE*, Ming-Chun Tien, and John E. Bowers, *Fellow, IEEE*

***Abstract*—In this letter, we present the design of an integrated optical isolator realized by bonding a silicon micro-ring resonator with a Ce:YIG garnet. The nonreciprocal phase shift effect induced by applying a radial magnetic field has been studied using the finite-element method; numerical results clearly point out how to optimize the thickness of the silicon ring and Ce:YIG garnet in order to maximize the nonreciprocal effect between the forward and backward TM modes.**

***Index Terms*—Finite-element method (FEM), integrated optics, isolators, magneto-optic material.**

I. Introduction

RECENT progress in the field of integrated optics has allowed an increasing number of devices to fit on the same chip. A very challenging component to be integrated with high performance is the optical isolator. Not only does it reduce the feedback optical noise in laser sources, but it also allows serial integration of different photonic components [1]. Several solutions have been proposed based on nonreciprocal radiation mode conversion [2], nonreciprocal losses (NRL) [3], interferometric configuration [4], and nonreciprocal phase shift (NRPS) [5], the latter of which comes out to be the more reliable for integrated isolators [6]. When a magnetic field is applied transversely to a waveguide made of magneto-optic (MO) material, the system is not reciprocal anymore and the forward and backward propagation constants are differentiated. Such isolators have been recently realized using MO photonic crystals and ring resonators. Although MO photonic crystals isolators have a very small footprint, they require either precise magnetization domain control over micron scale [7] or complex design of photonic crystals [8]. These issues make them difficult to be experimentally realized. A more promising solution is the use of nonreciprocal ring resonator, proposed by Kono *et al.* [9] and Jalas *et al.* [10]. However, the proposed structure is difficult to be implemented in practice, because of the tiny footprint. Recently, a TM isolator was demonstrated by bonding a silicon ring resonator with a cerium-substituted yttrium iron garnet (Ce:YIG) [6]. Combining the strong NRPS achievable in such material with the reduced size of a ring resonator, a small form factor integrated isolator was demonstrated with an isolation of 9 dB. In this letter we design and optimize this type of isolator at 1550 nm wavelength. By applying a radial magnetic field to the Ce:YIG, the clockwise (CW) and the counterclockwise (CCW) propagation constants for the TM mode will be significantly differentiated, resulting in a different resonant wavelength for the two directions. With a straight waveguide coupled to the ring (see Fig. 1(a)), the forward propagating light is coupled to the CW mode, while the backward light is coupled to the CCW mode. When the optical input is set off-resonance for the CW and on-resonance for the CCW, the forward light is transmitted while the backward light is filtered out by the ring, providing them the required isolation. The integrated isolator structure has been optimized using the Finite-Element Method (FEM), in terms of ring cross section and radius, in order to maximize the isolation.

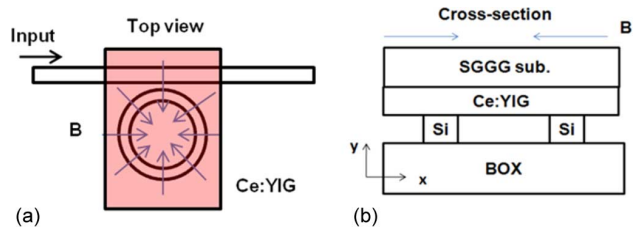

Fig. 1. Scheme of a ring isolator consisting of a ring resonator, a straight waveguide, and a bonded Ce:YIG layer. (a) Top view; (b) cross-section.

II. Theoretical Model

The isolator structure is shown in Fig. 1(b). A silicon ring resonator is fabricated on a silicon-on-insulator (SOI) wafer, having refractive index $n_{\mathrm{Si}} = 3.45$ and $n_{\mathrm{SiO2}} = 1.46$ respectively. The ring is bonded with a Ce:YIG garnet ($n_{\mathrm{Ce:YIG}} = 2.22$) grown on a (Ca,Mg,Zr)-substituted gadolinium gallium garnet (SGGG), ($n_{\mathrm{SGGG}} = 1.97$), whereas the remaining space is filled by air. Due to the high SOI index contrast, a high field confinement factor can be achieved even with rather small ring radius. To compute the modes and the effective index, we consider an equivalent straight waveguide with

$$\underline{E} = \left[E_x(x,y)\underline{i}_x + E_y(x,y)\underline{i}_y + jE_z(x,y)\underline{i}_z\right] e^{j\omega t - j\beta z} \quad (1.a)$$

$$\underline{H} = \left[H_x(x,y)\underline{i}_x + H_y(x,y)\underline{i}_y + jH_z(x,y)\underline{i}_z\right] e^{j\omega t - j\beta z} \quad (1.b)$$

and using the full vectorial FEM [11] we solve the curl-curl equation for the magnetic field $\underline{H}$

$$\nabla \times (\underline{\underline{K}}^{-1} \nabla \times \underline{H}) - k_0^2 \underline{H} = 0 \quad (2)$$

where $\underline{\underline{K}}$ is the relative permittivity tensor and k_0 is the wavenumber in vacuum. Similarly as in Jalas *et al.* [10], a correc-

Manuscript received March 31, 2011; revised July 21, 2011; accepted July 26, 2011. Date of publication August 22, 2011; date of current version October 21, 2011. This work was supported by DARPA MTO under CIPhER Contract HR0011-10-1-0079.

P. Pintus is with the University of California, Santa Barbara, CA 93106 USA, on leave from Scuola Superiore Sant'Anna, 56124, Pisa, Italy (e-mail: p.pintus@sssup.it).

M.-C. Tien and J. E. Bowers are with Department of Electrical and Computer Engineering, University of California, Santa Barbara, CA 93106 USA (e-mail: jtien@ece.ucsb.edu; bowers@ece.ucsb.edu).

Color versions of one or more of the figures in this letter are available online at http://ieeexplore.ieee.org.

Digital Object Identifier 10.1109/LPT.2011.2164397

1041-1135/$26.00 © 2011 IEEE

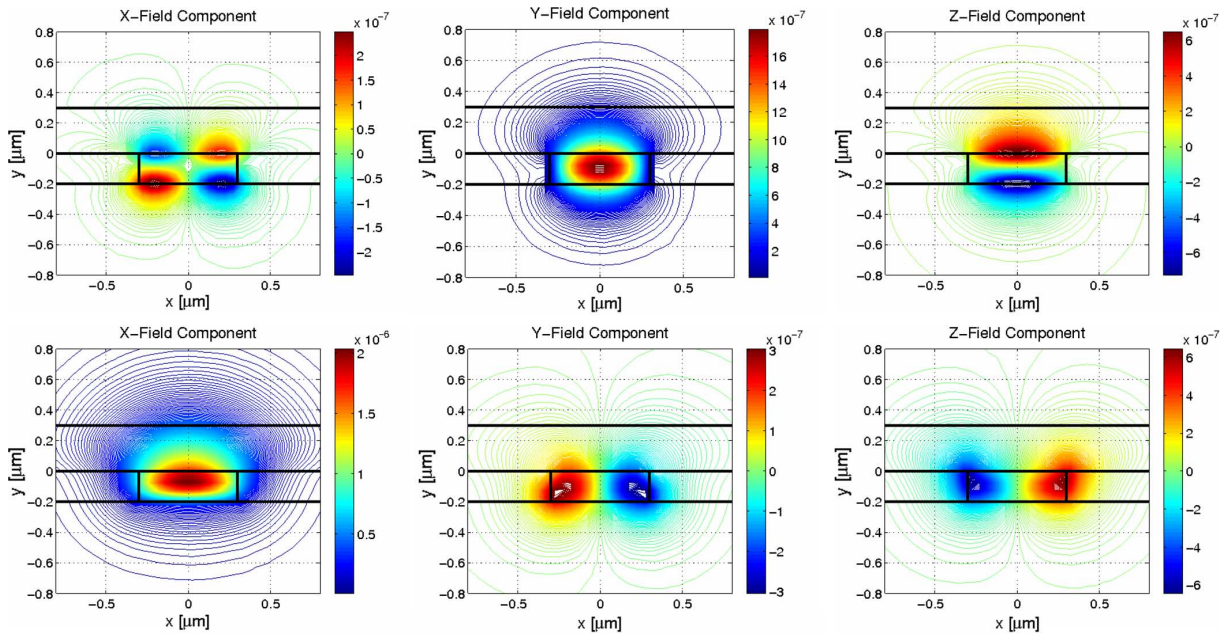

Fig. 2. Magnetic field H for the TE-mode (first row) and TM-mode (second row).

tion factor is applied for the fields, without significant change. By applying a static magnetic field along the radial direction (x-axis), the Ce:YIG permittivity tensor results in:

$$\underline{\underline{K}} = \begin{pmatrix} n^2 & 0 & 0 \\ 0 & n^2 & 0 \\ 0 & 0 & n^2 \end{pmatrix} + \begin{pmatrix} 0 & 0 & 0 \\ 0 & 0 & -j\varepsilon_{yz} \\ 0 & j\varepsilon_{yz} & 0 \end{pmatrix} \tag{3}$$

where ε_{yz} represents the MO effect and it is related to the Faraday rotation constant θ_F by $\varepsilon_{yz} = 2n_{\mathrm{Ce:YIG}}\theta_F/k_0$. In our case $\theta_F = 7 \cdot 10^{-3}$ rad/μm at $\lambda = 1550$ nm [6]. By implementing the node-based FEM with second order shape functions and introducing a penalty function to move out the spurious solutions [12], we got the quadratic eigenvalue problem [13]:

$$\left[\beta^2 \underline{\underline{M}} + \beta \underline{\underline{C}} + \underline{\underline{T}} - \omega^2 \underline{\underline{S}}\right] \underline{\hat{H}} = 0 \tag{4}$$

where $\underline{\underline{M}}$, $\underline{\underline{C}}$, $\underline{\underline{S}}$ and $\underline{\underline{T}}$ are sparse-matrices depending only on the geometry and the refractive index, and the entries of vector $\underline{\hat{H}} = (\underline{\hat{H}}_x^t, \underline{\hat{H}}_y^t, \underline{\hat{H}}_z^t)^t$ are the unknown magnetic field values at the interpolation nodes [11]. Equation (4) can be made explicit with respect to β by adding the equation $\underline{\hat{U}} = \beta \underline{\hat{H}}$ [13]:

$$\begin{pmatrix} \underline{\underline{0}} & \underline{\underline{I}} \\ -\underline{\underline{T}} + \omega^2 \underline{\underline{S}} & -\underline{\underline{C}} \end{pmatrix} \begin{pmatrix} \underline{\hat{H}} \\ \underline{\hat{U}} \end{pmatrix} = \beta \begin{pmatrix} \underline{\underline{I}} & \underline{\underline{0}} \\ \underline{\underline{0}} & \underline{\underline{M}} \end{pmatrix} \begin{pmatrix} \underline{\hat{H}} \\ \underline{\hat{U}} \end{pmatrix}. \tag{5}$$

By solving (5), the three components of the magnetic field and the effective refractive index ($n_{\mathrm{eff}} = \beta/k_0$) have been computed for the forward and backward propagating waves. TE and TM foward propagating modes are shown in Fig. 2. It can be seen that all three components are similar in magnitude for both polarizations, anyway the small ratio $\varepsilon_{yz}/n^2 \cong 0.015$ in the Ce:YIG and the short ring radius imply a negligible cross-polarization coupling via H_y (TE) with H_z (TM) or vice-versa.

The resonance wavelengths must satisfy the phase condition

$$2\pi R n_{eff}^{\pm}(\lambda^{\pm}) = m\lambda^{\pm} \tag{6}$$

where m is an integer, and $\pm$ indicate the CW and CCW resonant wavelengths respectively. From (6) the resonance wavelength splitting can be estimated as $\Delta\lambda = |\lambda^+ - \lambda^-| = \lambda\Delta n_{\mathrm{eff}}/n_g$, where n_g is the average group index with respect to the two directions. It is worth noting that for maximizing the optical isolation, the minimal radius of the ring should be chosen so that the transmission spectra for the forward and backward resonances are offset at least by half of the free spectral range (FSR). It means $FSR = \lambda^2/(2\pi R n_g) = 2\Delta\lambda$. Once the resonance wavelength splitting is computed, the minimal ring radius is identified. For larger radii the $(n+1)$th order CCW resonance peak results to be closer to the nth CCW resonance peak, reducing the isolation ratio. At the limit that the CW resonance peak overlaps with the higher order CCW resonance peak (e.g. FSR $= \Delta\lambda$), the isolation is zero. To quantitatively estimate the isolation, we model the ring-waveguide system with the following equations [14], [15]:

$$\frac{d}{dt}a_c^{\pm}(\omega) = \left[i\omega_0^{\pm} - \left(\frac{\gamma_0}{2T} + \frac{\kappa(\omega)}{2T}\right)\right] a_c^{\pm}(\omega) + i\frac{\sqrt{\kappa(\omega)}}{T} a_{in}(\omega) \tag{7.a}$$

$$a_t^{\pm}(\omega) = \sqrt{1-\kappa(\omega)}\, a_{in}(\omega) + i\sqrt{\kappa(\omega)}\, a_c^{\pm}(\omega) \tag{7.b}$$

where $\omega_0^{\pm}$ are the ring resonance frequencies, a_c, a_{in}, and a_t denote the field in the cavity, the input field in the waveguide and the transmitted field, respectively. Moreover κ and γ_0 are the power coupling ratio and the intrinsic cavity loss during one round trip time, which is denoted as $T = 2\pi R/v_g$, being v_g the group velocity. If the input optical field is sinusoidal $a_{\mathrm{in}} \sim \exp(i\omega t)$, then the transfer function between $a_t^{\pm}$ and a_{in} is

$$a_t^{\pm}(\omega) = \frac{\sqrt{1-\kappa(\omega)}\left[i\left(\omega-\omega_0^{\pm}\right) + \frac{\gamma_0}{2T} + \frac{\kappa(\omega)}{2T}\right] - \frac{\kappa(\omega)}{T}}{\left[i\left(\omega-\omega_0^{\pm}\right) + \frac{\gamma_0}{2T} + \frac{\kappa(\omega)}{2T}\right]} a_{in}(\omega). \tag{8}$$

The isolation is then computed as $\left|a_t^+(\omega_0^-)/a_t^-(\omega_0^-)\right|^2$. It is now useful to recall the definition of the unloaded resonator quality

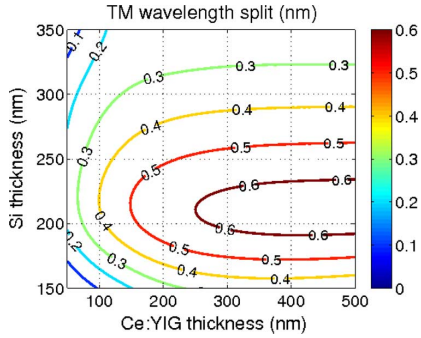

Fig. 3. TM wavelength split with respect to Si and Ce:YIG layer thicknesses.

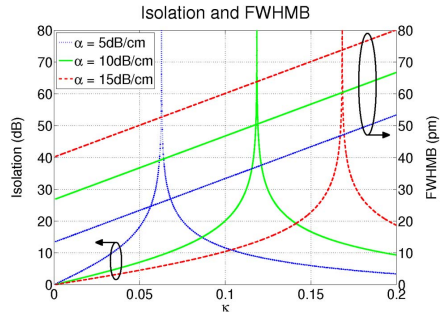

Fig. 4. Isolation and FWHMB as functions of the coefficient κ.

factor $Q_0 = \omega_0 T/\gamma_0 = \omega_0/\alpha v_g$, where α is the loss coefficient, and the definition of the coupling quality factor $Q_c = \omega_0 T/\kappa$, which are used to estimate the full width at half maximum bandwidth (FWHMB) as $\lambda_0/Q_{\rm tot}$, where λ_0 is the resonant wavelength and $Q_{\rm tot} = Q_0 Q_c/(Q_0 + Q_c)$.

III. Numerical Results

In order to guarantee single mode regime, we have considered a 600-nm wide silicon ring. The thickness of the silicon ring and of the Ce:YIG layer have been chosen to maximize the resonance wavelength split $(\Delta\lambda)$ between the two propagation directions. Simulations have been done for different layer thicknesses and the results have been interpolated using cubic spline method. Contour plots of the $\Delta\lambda$ are shown in Fig. 3. We can clearly see that by increasing the Ce:YIG layer thickness from 100 nm up to 350 nm, the mode, which is mainly confined in the silicon, expands to the MO material, increasing the NRPS effect. Thicker Ce:YIG-layer does not increase the split because the field is more confined in the silicon. Vice-versa, the maximum split can be reached when the silicon thickness is 215 nm. The NRPS is maximized when the maximum of $|H_x|^2$ is located close to the boundary of the two materials. The same calculation for the TE mode shows a negligible split for CW and CCW propagating TE waves. For a Ce:YIG thickness equals to 350 nm and a ring thickness of 215 nm, we computed $\Delta\lambda = 0.63$ nm. Imposing FSR $= 1.26$ nm, we found a minimal radius $R = 92.5$ μm, which can be used to calculate the isolation and the FWHMB of the isolator reported in Fig. 4. The external magnetic flux density needed to saturate the Ce:YIG is $\sim$50 Gauss and can be applied with a permanent magnet [6].

The coefficient κ is a crucial issue for ring-waveguide systems because it is related to the ring-waveguide distance and it is difficult to be experimentally controlled with high accuracy. Considering several values for the loss coefficient α, the isolator shows different optimum values for κ (Fig. 4), following the resonance coupling condition $\kappa \sim \gamma_0$. Note that a variation up to 15% from the optimum κ can still guarantee an isolation higher than 20 dB. From Fig. 4, it appears that the higher loss allowed a larger FWHMB, which is correct for γ_0 smaller than 1. On the other hand, higher ring loss implies higher insertion loss and high magneto-optic effect needed (higher Faraday coefficient or magnetic field). The isolation bandwidth can be increased using cascaded ring resonators with similar structures [9], while thermal tuning can be used to align the isolation bandwidth with the laser wavelength.

IV. Conclusion

In this work we have numerically demonstrated the design of integrated optical isolators based on bonding of a silicon ring resonator with a nonreciprocal MO garnet using FEM. The compact device has a high isolation in spite of nonideal coupling. Finally, in order to overcome the bandwidth limitation and further enhance the isolation, cascaded ring resonators can be used.

Acknowledgment

The authors thank H. Kroemer, T. Mizumoto, S. Rodgers, and D. Awschalom for helpful discussions.

References

[1] T. R. Zaman, X. Guo, and R. J. Ram, "Semiconductor waveguide isolators," *J. Lightw. Technol.*, vol. 26, no. 2, pp. 291–301, Jan. 15, 2008.
[2] T. Shintaku, "Integrated optical isolator based on efficient nonreciprocal radiation mode conversion," *Appl. Phys. Lett.*, vol. 73, no. 14, pp. 1946–1948, 1998.
[3] W. Van Parys, B. Moeyersoon, D. Van Thourhout, R. Baets, M. Vanwolleghem, B. Dagens, J. Decobert, O. Le Gouezigou, D. Make, R. Vanheertum, and L. Lagae, "Transverse magnetic mode nonreciprocal propagation in an amplifying AlGaInAs/InP optical waveguide isolator," *Appl. Phys. Lett.*, vol. 88, no. 7, pp. 071115–071115-3, 2006.
[4] T. R. Zaman, X. Guo, and R. J. Ram, "Proposal for a polarization-independent integrated optical circulator," *IEEE Photon. Technol. Lett.*, vol. 18, no. 12, pp. 1359–1361, Jun. 15, 2006.
[5] J. Fujita, M. Levy, R. M. Osgood, L. Wilkens, and H. Dotsch, "Waveguide optical isolator based on Mach–Zehnder interferometer," *Appl. Phys. Lett.*, vol. 76, no. 16, pp. 2158–2160, 2000.
[6] M.-C. Tien, T. Mizumoto, P. Pintus, H. Kromer, and J. E. Bowers, "Silicon ring isolators with bonded nonreciprocal magneto-optic garnets," *Opt. Express*, vol. 19, no. 12, pp. 11740–11745, 2011.
[7] Z. Wang and S. Fan, "Optical circulators in two-dimensional magneto-optical photonic crystals," *Opt. Lett.*, vol. 30, pp. 1989–1991, 2005.
[8] W. Śmigaj, J. Romero-Vivas, B. Gralak, L. Magdenko, B. Dagens, and M. Vanwolleghem, "Magneto-optical circulator designed for operation in a uniform external magnetic field," *Opt. Lett.*, vol. 35, pp. 568–570, 2010.
[9] N. Kono, K. Kakihara, K. Saitoh, and M. Koshiba, "Nonreciprocal microresonators for the miniaturization of optical waveguide isolators," *Opt. Express*, vol. 15, no. 12, pp. 7737–7751, 2007.
[10] D. Jalas, A. Petrov, M. Krause, J. Hampe, and M. Eich, "Resonance splitting in gyrotropic ring resonators," *Opt. Lett.*, vol. 35, pp. 3438–3440, 2010.
[11] A. Konrad, "High-order triangular finite elements for electromagnetic waves in anisotropic media," *IEEE Trans. Microw. Theory Tech.*, vol. MTT-25, no. 5, pp. 353–360, May 1977.
[12] B. A. Rahman and J. B. Davies, "Penalty function improvement of waveguide solution by finite elements," *IEEE Trans. Microw. Theory Tech.*, vol. MTT-32, no. 8, pp. 922–928, Aug. 1984.
[13] F. Tisseur and K. Meerbergen, "The quadratic eigenvalue problem," *SIAM Rev.*, vol. 43, pp. 235–286, 2001.
[14] M. L. Gorodetsky, A. D. Pryamikov, and V. S. Ilchenko, "Rayleigh scattering in high-Q microspheres," *J. Opt. Soc. Amer. B*, vol. 17, pp. 1051–1057, 2000.
[15] T. J. Kippenberg, S. M. Spillane, and K. J. Vahala, "Modal coupling in traveling wave resonators," *Opt. Lett.*, vol. 27, pp. 1669–1671, 2002.